Quantifying the impact of soft surface soil layers on fault rupture propagation and kinematic distress of offshore and onshore pipelines

by

Nikolaos MAKRAKIS[1], Prodromos N. PSARROPOULOS[2]
Anastasios SEXTOS[3], Yiannis TSOMPANAKIS[1*]

[1]Technical University of Crete, Greece
[2]National Technical University of Athens, Greece
[3]University of Bristol, United Kingdom

ABSTRACT

Offshore and onshore natural gas pipelines constitute critical facilities that often cross seismic prone regions, thus, they are exposed to earthquake-induced Permanent Ground Displacements (PGDs). The excessive PGDs that are often developed in the vicinity of a fault scarp may affect pipeline integrity and safe functioning. On the other hand, the complete avoidance of fault rupture zones may be economically and technically unfeasible. Pipelines subjected to PGDs usually exhibit large levels of strains, and consequently they may experience local buckling and even rupture failures. For this reason, the impact of overburden soil layers on the propagation of tectonic faulting to the surface and the developed PGDs is crucial for the reliable assessment of pipeline distress.

This study investigates numerically the complex phenomenon of seismic fault rupture propagation from base rock to surface, focusing on the problem of fault-pipeline intersection. The main aim is to correlate earthquake magnitude with: (i) the critical engineering parameter of ground surface inclination with respect to the developed PGDs, and (ii) the associated kinematic distress of pipelines in terms of strains. In this light, a decoupled Finite Element (FE) modeling approach is adopted, consisting of two separate numerical models for the simulation of soil and pipeline response. Furthermore, soil non-linearities are taken into account utilizing Mohr-Coulomb constitutive model with isotropic strain softening. A detailed parametric investigation has been performed considering various loading conditions (directly related to earthquake magnitude), different faulting mechanisms and dip angles, as well as overlying soil properties. Accordingly, useful conclusions are derived that can be utilized in the preliminary seismic design of offshore and onshore pipelines against fault rupture.

1. INTRODUCTION

Fault rupture propagation to ground surface has attracted considerable research interest recently. The impact that various critical parameters (e.g., fault type and dip angle, overburden soil thickness and properties) may have on fault rupture patterns has been investigated in field studies (Bray et al., 1994), numerical (Loukidis et al., 2009; Thebian et al., 2018), as well as experimental investigations (Chang et al., 2015).

However, the critical engineering parameter of ground surface inclination due to fault rupture propagation has not been investigated so far. In addition, very few publications correlate analytically the earthquake magnitude with tectonic characteristics (e.g., bedrock displacement) and rupture parameters (e.g., surface rupture length), either with (Turgut et al., 2017) or without (Bonilla et al., 1984; Wells and Coppersmith, 1994) taking into account the presence of soft soil layer(s) that lie over the rigid bedrock.

Gas transmission pipelines often cross extensive geohazardous areas and consequently, they are extremely vulnerable to PGDs due to tectonic faulting. Several case studies have been reported demonstrating severe damages of pipeline networks, worldwide (Nair et al., 2018). However, the fact that the complete avoidance of fault rupture areas might not be feasible from an economic and/or technical perspective, highlights the necessity for an accurate and realistic assessment of pipeline distress due to PGDs. Along these lines, extensive research has been conducted to investigate the problem of fault-pipeline intersection, analytically (Karamitros et al., 2011, 2007; Kennedy et al., 1977; Newmark and Hall, 1975) experimentally (Jalali et al., 2018; Tsatsis et al., 2019) and numerically (Fadaee et al., 2020; Joshi et al., 2011). It is worth noting that some of the above methodologies have been adopted by several guidelines for seismic design of pipelines (e.g., ALA, 2001; EC8, 2006).

However, most of the previous studies have investigated the problem of fault-pipeline intersection assuming that the pipeline is (rather unrealistically) laid directly on the bedrock, thus neglecting the effect of overlying soil stratum beneath the pipeline, which could considerably influence the pipeline's response. Additionally, the correlation, in terms of strains, between the main parameters of the tectonic rupture and pipeline kinematic distress has not yet been investigated.

Based on the above, the main aim of the current study is to develop a new empirical approach for correlating the earthquake magnitude (which is directly related to the fault offset at the bedrock) with: (i) the resulting ground surface inclination due to fault rupture propagation, in terms of PGDs, and (ii) the associated pipeline structural response, as expressed in terms of strains. For this purpose, a decoupled FE modeling approach is adopted, consisting of two separate models, for the simulation of soil and pipeline response, respectively. Soil non-linearity is considered by means of Mohr-Coulomb constitutive model with isotropic strain softening. Initially, the proposed numerical models are validated against previous experimental studies. Next, a refined parametric investigation is performed, examining both normal and reverse faults at several dip angles. Since the bedrock dislocation is directly associated with the magnitude, different earthquake magnitudes are considered. Moreover, a sandy soil stratum is assumed on top of the rigid bedrock, examining various combinations of material properties and layer thickness. The obtained results are used to establish empirical relationships that can be efficiently applied in engineering practice for a preliminary estimate of the pipeline seismic demand (i.e., strains in this case) with earthquake magnitude.

2. PROBLEM DESCRIPTION

Earthquake fault rupture leads to an abrupt dislocation of rock outcrops at the surface. Subsequently, adjacent structures and pipelines, which are assumed to be laid directly on the (bed)rock, are exposed to excessive deformations, as illustrated in Figure 1a. However, in reality, rigid bedrock is usually covered by soft soil deposits ranging from tens to thousands of meters depending on local site conditions. Therefore, once the rupture initiates, the aforementioned dislocation often propagates towards the ground surface through overlying soil layer(s), affecting buried or aboveground pipelines, and leading to an inclined surface, as shown in Figure 1b.

Figure 1. Fault rupture and fault-pipeline intersection: a) without, and b) with the presence of soil overburden.

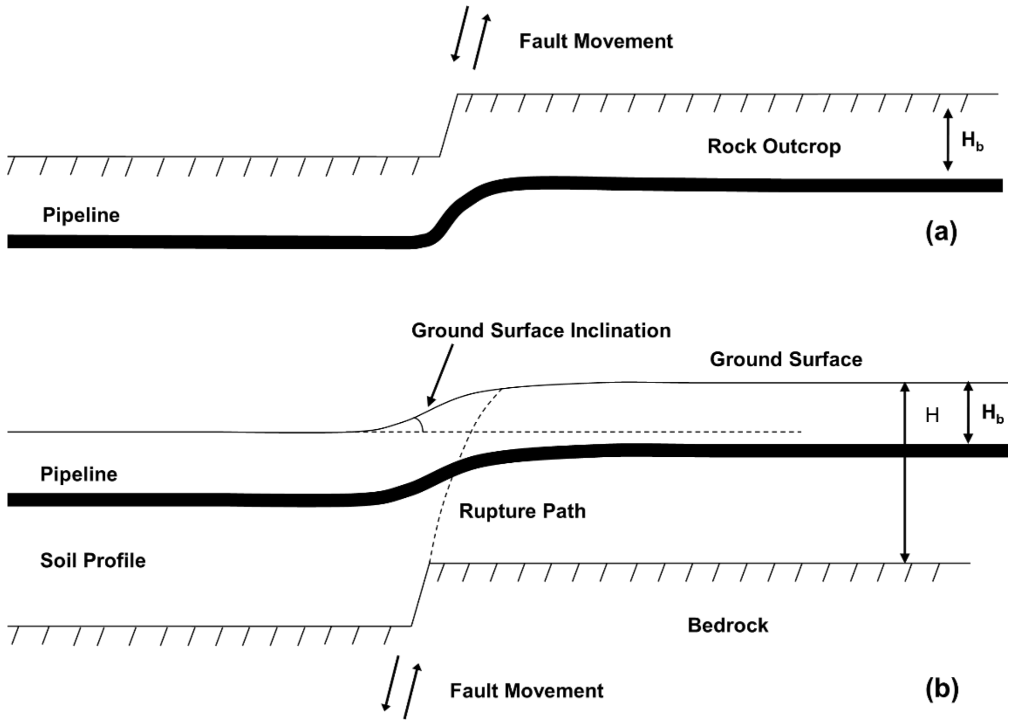

The assumption made in this paper for relating the Average bedrock Displacement, *AD*, with earthquake moment magnitude, *M* is based on the following expression, that was proposed by Wells and Coppersmith (1994) for both normal and reverse faults:

$$log(AD) = a + b \cdot M \quad (1)$$

where, *α* and *b* are regression coefficients equal to -4.80 and 0.69, with 0.36 standard deviation, as well as 0.57 and 0.08 standard errors, respectively. Moment magnitude ranges from 5.6 to 8.1, while *AD* varies between 0.05 m and 8.0 m, as shown in Figure 2. Note that Average Displacement describes the mean bedrock displacement observed along the fault rupture plane.

Figure 2. Average bedrock displacement in terms of earthquake moment magnitude (Wells and Coppersmith,1994).

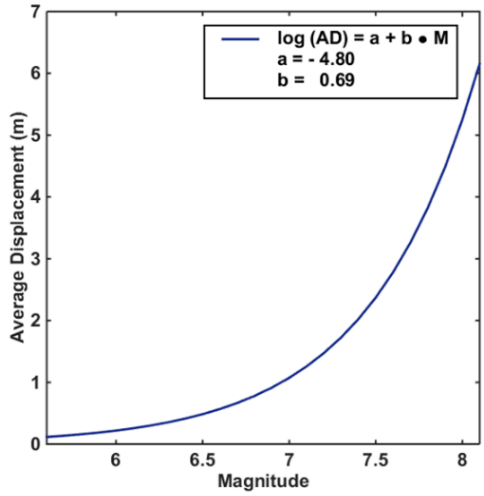

3. NUMERICAL MODELING OF SOIL RESPONSE

Soil response due to fault rupture is simulated utilizing ABAQUS software (Simulia, 2014) with quasi-static analyses. Figure 3 presents a uniform soil bed of thickness, *H*, located on top of the rigid bedrock. As shown in Figure 3a, the width, *B*, of the FE domain is considerably larger than the soil stratum thickness, *H*, (i.e., *B* = *4H*) aiming to minimize undesirable boundary effects (Bray, 1990). Nevertheless, wider FE models (i.e., *B* = *8H*) have been used for the cases of normal faults consisting of 50m and 100m-thick soil layers, as well as for reverse faults, regardless of soil layer thickness.

Soil layer is simulated in 2D plane-strain conditions using four-node quadrilateral elements (type CPE4 in ABAQUS). An optimal numerical performance is achieved adopting a coarser FE mesh discretization at the edges of the model and a finer FE mesh in the vicinity of the failure plane (Anastasopoulos et al., 2007). Indicatively, Figure 3 displays the dimensions of the FE mesh for the 50m-thick overlying soil deposit.

The numerical analysis is performed in two steps: (a) geostatic, where gravity force is applied to the model, and (b) fault displacement, where bedrock dislocation is imposed. In particular, a differential displacement at a predetermined angle, *α*, parallel to the fault plane is applied to the left vertical phase and bottom nodes of the FE model (hanging wall). The bottom nodes of the foot wall are fixed, whereas roller boundary conditions are imposed on the right vertical phase of the FE model. Figures 3a and 3b demonstrate the boundary and loading conditions regarding normal and reverse faulting, respectively.

3.1. Soil constitutive model for sand

Several researchers (e.g., Anastasopoulos et al. (2007), Oettle and Bray (2017)) have shown that the soil strain softening plays a key role in the reliable numerical modeling of soil non-linearities. Herein, the elastoplastic Mohr-Coulomb constitutive model with isotropic strain softening is utilized, as introduced by Anastasopoulos et al. (2007).

Figure 3. FE numerical model of: a) normal, and b) reverse fault.

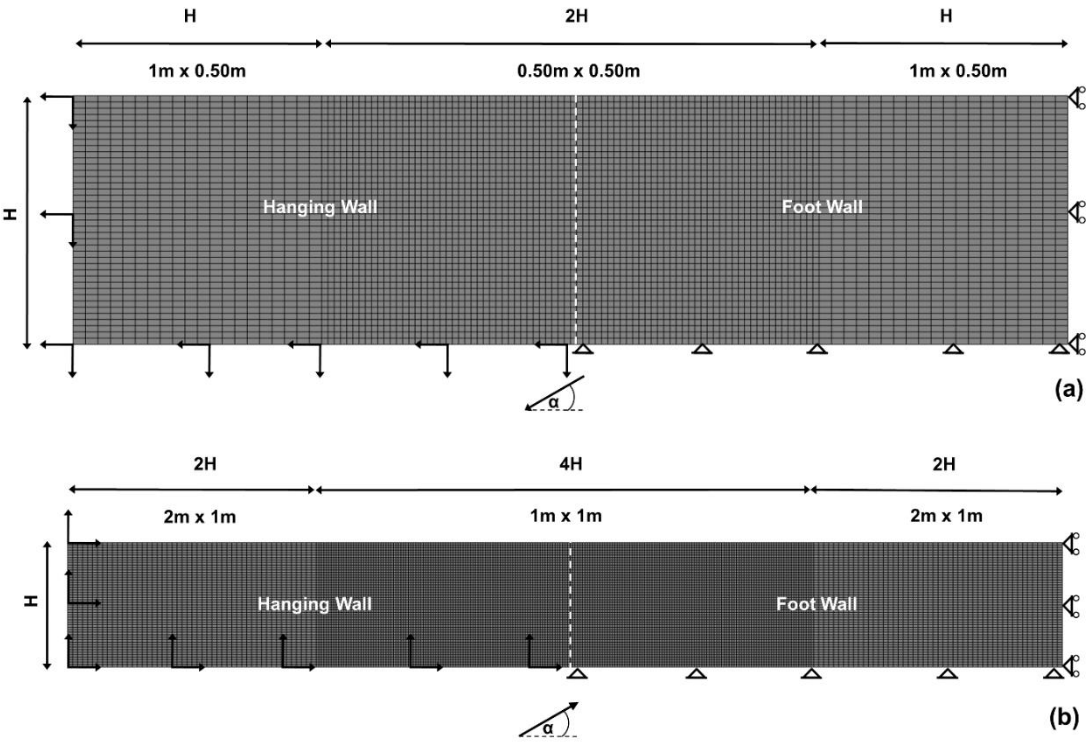

The pre-yield behavior of soil is assumed to be elastic and is defined in terms of the secant shear modulus, *G*, whereas, Mohr-Coulomb failure criterion is used to define the post-peak soil behavior. An isotropic strain softening law is applied, where the mobilized friction and dilation angles are linearly decreased as the octahedral plastic shear strain, (i.e., γ^{p}_{oct}) increases, as follows:

$$\varphi = \begin{cases} \varphi_p - \frac{\varphi_p - \varphi_{res}}{\gamma_f^p}\gamma_{oct}^p & for \quad 0 \leq \gamma_{oct}^p < \gamma_f^p \\ \varphi_{res} & for \quad \gamma_{oct}^p \geq \gamma_f^p \end{cases} \tag{2}$$

$$\psi = \begin{cases} \psi_p \left(1 - \frac{\gamma_{oct}^p}{\gamma_f^p}\right) & for \quad 0 \leq \gamma_{oct}^p < \gamma_f^p \\ \psi_{res} & for \quad \gamma_{oct}^p \geq \gamma_f^p \end{cases} \tag{3}$$

where, φ and ψ denote the friction and dilation angles, respectively. Moreover, φ_p and φ_{res} represent the ultimate mobilized (peak) and residual friction angles, respectively, whereas ψ_p and ψ_{res} denote the corresponding dilation angles. In addition, γ^{p}_{f} expresses the failure plastic octahedral shear strain at the end of strain softening. The aforementioned constitutive model has been implemented in ABAQUS software via a user-developed subroutine by authors' group (Chatzidakis et al., 2022).

3.2. Validation against experimental results

The proposed numerical model has been validated in order to verify its reliability and accuracy based on a 100g centrifuge test that was conducted at the University of Dundee by Anastasopoulos et al. (2007). In this case, an overburden soil layer of height, $H = 25\ m$, consisting of medium-dense Fontainebleau sand with relative density $Dr = 80\ \%$ was subjected to both normal and reverse fault motion dipping at $\alpha = 60^o$. Detailed presentation of the numerical model and the corresponding experimental results can be found in the recent paper by Chatzidakis et al. (2022).

A wide range for bedrock offset has been examined, corresponding to *D = 0.25, 0.5, 0.85 and 1.08 m* and *D = 0.18, 0.49, 0.7, and 1.13 m* for normal and reverse faults, respectively. As it has been shown by Chatzidakis et al. (2022), in general, the numerical results are in good agreement with the experimental results, in terms of ground-surface vertical displacements, *dz*, regardless of fault type, especially for low levels of bedrock offset. Nonetheless, minor differences have been observed for large bedrock dislocations.

4. NUMERICAL MODELING OF PIPELINE RESPONSE

ABAQUS finite-element computer software has been employed to simulate the pipeline response due to fault rupture. More specifically, the pipeline has been simulated utilizing two-node PIPE21 beam elements, which are commonly used, since they allow transverse shear deformation. Pipeline-soil and pipeline-bedrock interaction are modeled using the four-node PSI24 interface elements, where the one side of the element represents the ground or bedrock surface and the other side is attached to the examined pipeline. Soil resistance is assessed based on pipeline's embedment depth, friction angle, unit weight, etc., according to ALA guidelines (ALA, 2001).

Figure 4 depicts the numerical model of the pipeline. In particular, the relative PGDs that have been derived from the soil model along the pipeline's embedment depth, H_b, are imposed on the pipeline through the PSI elements. A pipeline of a typically infinite length has been used to avoid undesired boundary effects at the edges of the model. Moreover, the ends of the pipeline and the soil surface nodes towards the foot wall block are fixed.

Figure 4. FE numerical model of the pipeline.

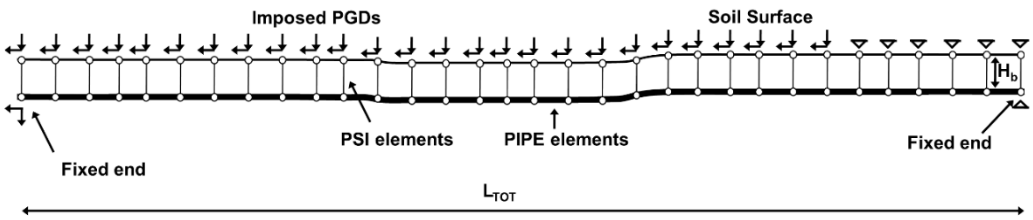

4.1. Validation with experimental results

The pipeline FE model is compared with the experimental investigation of Tsatsis et al. (2019) for normal and reverse faulting. Dense Longstone sand with $D_r = 90\%$ was used in the experiments with dry unit weight equal to $\gamma = 15.68\ kN/m^3$. The (scaled) pipe had a diameter of $D = 35\ mm$, a thickness of $t = 0.5\ mm$ and consisted of stainless steel grade AISI Type 444. The pipe burial depth was equal to $H_b = 0.55\ m$, measured from its centerline. Detailed presentation of the numerical model and the corresponding experimental results have been presented by Chatzidakis et al. (2022).

The numerical and experimental results are compared with respect to four different normalized vertical bedrock movements: *D / H = 0.5, 1, 1.5* and *2*, in terms of the invert axial strain, $\varepsilon_{a,invert}$, i.e., the axial strain in the pipeline's bottom line. The results reported by Chatzidakis et al. (2022) reveal that for normal faults, the proposed numerical model slightly overestimates the tensile strains, while the compressive strains are accurately derived. In the case of reverse faulting, both the compressive and the tensile strains are slightly overestimated.

5. NUMERICAL RESULTS

In the sequence, characteristic results are presented from an extensive parametric investigation, in which several critical factors that may affect fault rupture propagation have been examined. Both normal and reverse faults with dip angles $\alpha = 30^o$ and 60^o are simulated. Three values of bedrock dislocation, *D = 0.48 m, 1.07 m* and *2.37 m* are considered, which according to Equation (1), correspond to earthquake magnitude equal to *M = 6.5, 7.0* and *7.5*, respectively. A uniform soil stratum of *H* ranging from *5* to *100 m* is considered, consisting of three idealized sand types, namely Loose Sand (LS), Medium Sand (MS) and Dense Sand (DS). Table 1 summarizes the soil properties, where it is noted that Elastic Modulus varies with depth, *E(z)*. Moreover, φ_{res} and ψ_{res} are set equal to 30^o and 0^o, respectively, regardless of sand type.

Table 1. Soil properties.

Sand	**Soil Density P (t/m^3)**	**Elastic Modulus E(z) (MPa)**	**Poisson's ratio V (-)**	**Friction angle φ_{pl} – φres (^{o})**	**Dilation angle ψ_{pl} - ψ_{res} (^{o})**
Loose	1.6	5 + 0.75 z	0.33	30	0
Medium	1.8	10 + 1.5 z	0.33	34 – 30	6 – 0
Dense	2.0	20 + 3 z	0.33	39 – 30	11 – 0

The pipeline is considered to have outer diameter, *D = 2R = 0.914 m* (*36 in*), wall thickness, *t = 19.05 mm* (*0.75 in*), (*R / t = 24*) and total length of a few kilometers depending on the length of the examined soil deposit (e.g., *4 km* for *80 m* soil stratum). The typical API 5L X65 steel grade has been chosen, characterized by a bilinear elastic-plastic stress-strain curve (*E = 210 GPa*, *v = 0.3*, yield stress, σ_1, equal to *450 MPa* and failure stress, σ_2, equal to *530 MPa*). Pipeline-soil interaction is considered by means of the critical state of friction angle and the coefficient of lateral earth pressure at rest, K_0, which is set equal to *0.5*. With respect to external pipe coating, the friction coefficient, *f*, has been set equal to *0.7*, corresponding to smooth steel. Moreover, the pipeline's burial depth, H_b, is set equal to *2 m*, calculated from its centerline.

Fault rupture propagation is investigated in terms of: i) PGDs at ground surface, with respect to the ratio *x / H*, where *x* is the location along the FE soil cover, and ii) the plastic deformation of the FE rupture planes. PGDs are represented with respect to *d* = $\sqrt{d^2x + d^2y}$, where *dx* and *dy* respectively denote the differential lateral and vertical ground displacements induced by bedrock faulting. Fault-pipeline intersection is examined in terms of *x / H* and pipeline maximum (i.e., tensile) and minimum (i.e., compressive) strains, in order to be comparable with existing limit state criteria (e.g., EC 8 Part 4 and ALA). Herein, the results refer to the compressive strains, since API 5L X65 has been considered more sensitive to compression than tension. It is noted that due to space limitations, a reference case model is presented herein, with $\alpha = 30^o$, $M = 7.0$, $H = 20\ m$.

5.1 Impact of soil layer properties

The impact of soil layer properties is presented in this section. Figure 5 illustrates that failure patterns of antithetic inclination reach ground surface for the case of normal faulting, regardless of sand type. In contrast, according to Figure 6, this is not the case for reverse faults. Regarding sand type, more abrupt displacements and higher plastic strains are observed for DS, compared to MS and LS, regardless of fault type. In addition, a wider distortion zone is developed at the ground surface for normal faulting and LS, compared to MS and DS. These findings can be attributed to the lower stiffness that characterize LS, which leads to higher levels of elastic deformation.

On the other hand, Figure 7 demonstrates that the pipeline buried into LS experiences lower strains, compared to MS and DS for all the examined cases. Additionally, due to the existence of the sandy layer, considerably lower strain levels are observed when the pipeline is laid on top of the sandy layer (continuous curves) compared to the case that it is directly laid on the bedrock (dashed curve), as shown in Figure 1a. This trend is more pronounced for reverse faulting.

Figure 5. Impact of soil properties on normal faulting propagation: a) PGDs, and b) plastic deformations.

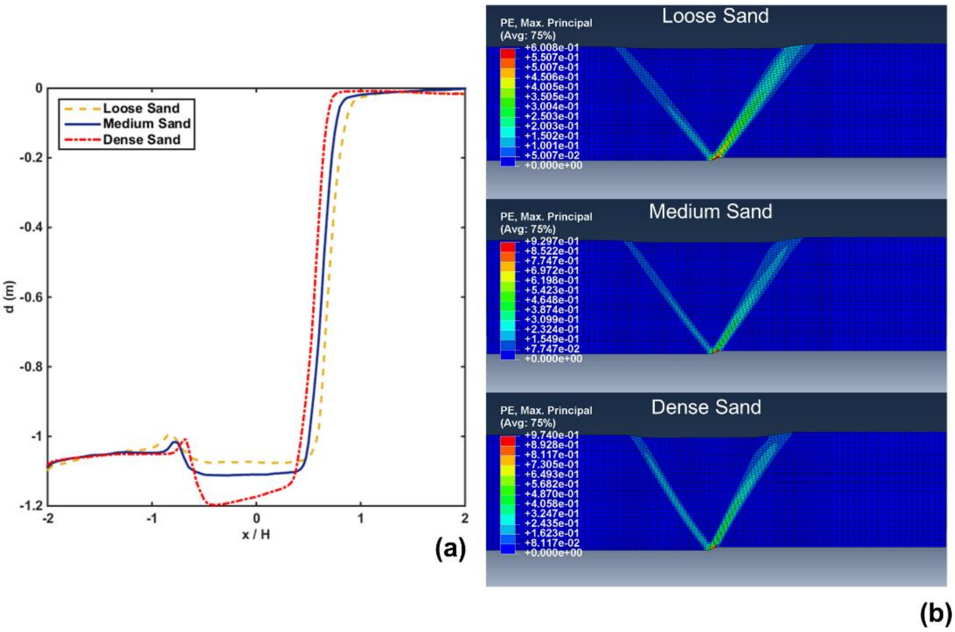

Figure 6. Impact of soil properties on reverse faulting propagation: a) PGDs, and b) plastic deformations.

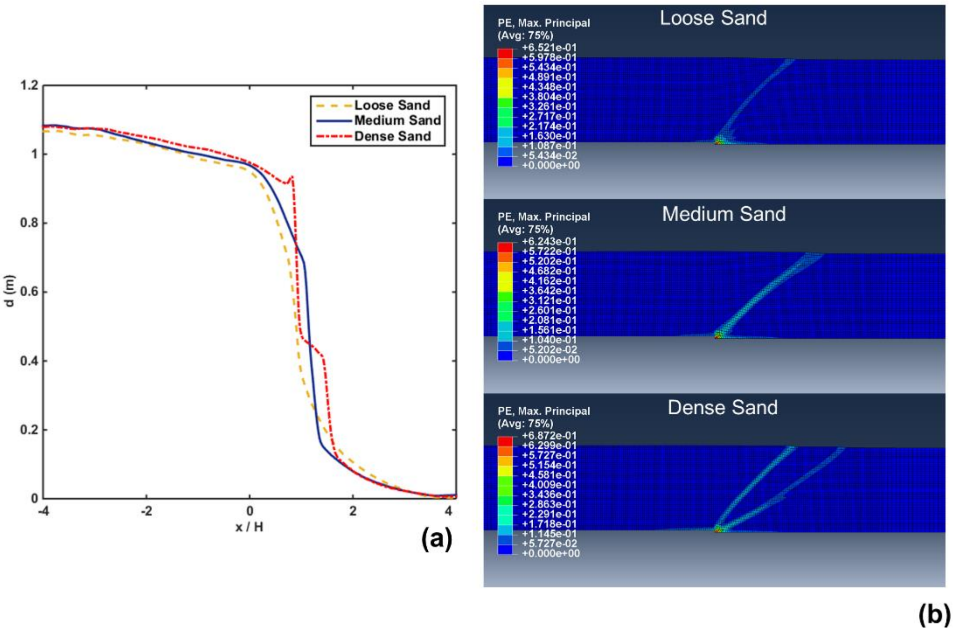

Figure 7. Impact of soil properties on compressive strains for: a) normal, and b) reverse faults.

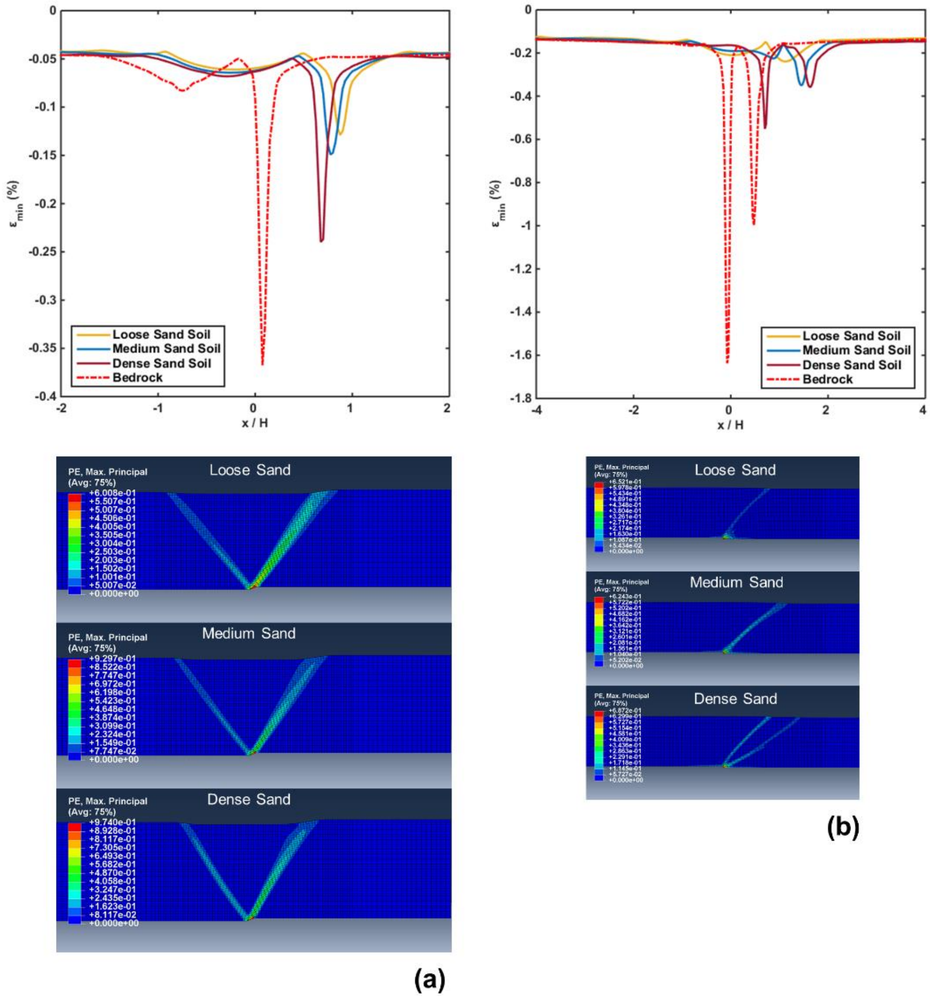

5.2 Ground surface inclination and empirical correlations

The deformed FE models derived from ABAQUS software are used to evaluate the critical engineering parameter of ground surface inclination. After plotting the resulting inclination values, the two-parameter-exponential-distribution has been selected as it can accurately correlate the derived data, which is expressed by the following equation:

$$f(x) = a \cdot e^{bx} \tag{4}$$

where, *f(x)* is the normalized ratio *D / H*, *α* and *b* are defined as coefficients with *95 %* confidence bounds, and x denotes the parameter of ground surface inclination.

According to Figure 8, LS leads to lower ground surface inclination, compared to MS and DS, regardless of earthquake magnitude, dip angle and fault type. Regarding dip angle, $\alpha = 30^o$ results in higher ground surface inclination, compared to $\alpha = 60^o$, for normal faulting. However, this trend is not observed for reverse faults, in which, as illustrated in Figure 9, soil deposits of $H \geq 20\ m$ present a significant decrease of ground surface inclination for all the examined dip angles and earthquake magnitudes. On the other hand, reverse faulting tends to produce higher ground surface inclination than normal faulting for thinner soil deposits and high earthquake magnitudes.

Figure 8. Surface inclination for normal faulting: a) LS, b) MS, and c) DS.

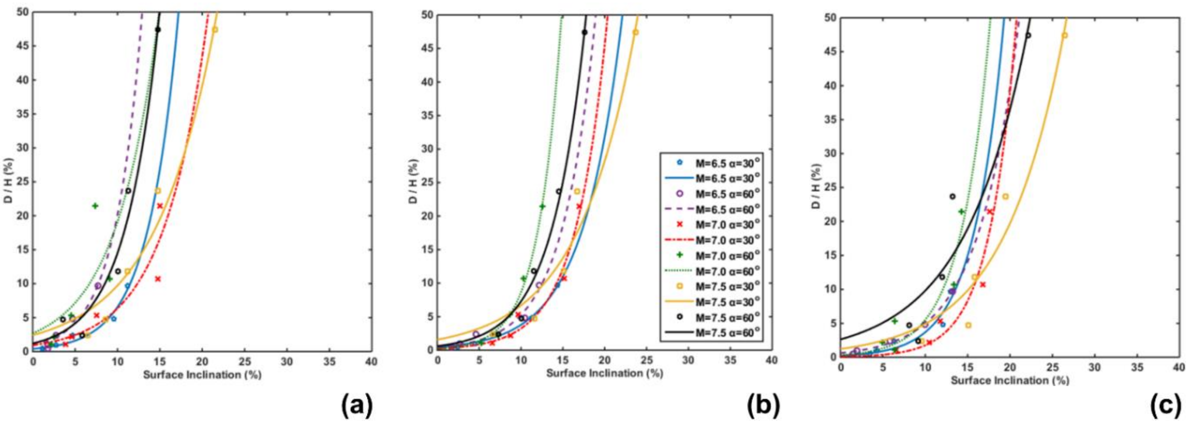

Figures 10 and 11 display the maximum absolute values of compressive strains with respect to earthquake moment magnitude. In general, higher strain levels are observed for DS compared to MS and LS, regardless of fault type and dip angle values. Figure 10 illustrates that LS and MS result in allowable compressive strains regardless of earthquake magnitude values, for normal fault dipping at $\alpha = 60^o$. Conversely, Figure 11 depicts the excessive compressive strains that exceed allowable limits, which are developed for *M = 7.0* and when the pipeline is laid directly on bedrock (no backfill) or is buried inside a 5m-thick soil cover, regardless of sand type and dip angle values. It is noted that the excessive reverse fault offset corresponding to *M = 7.5* leads to the exceedance of compressive strength capacity of the examined pipe cross-section and API 5L X65 steel grade material.

Figure 9. Surface inclination for reverse faulting: a) LS, b) MS, and c) DS.

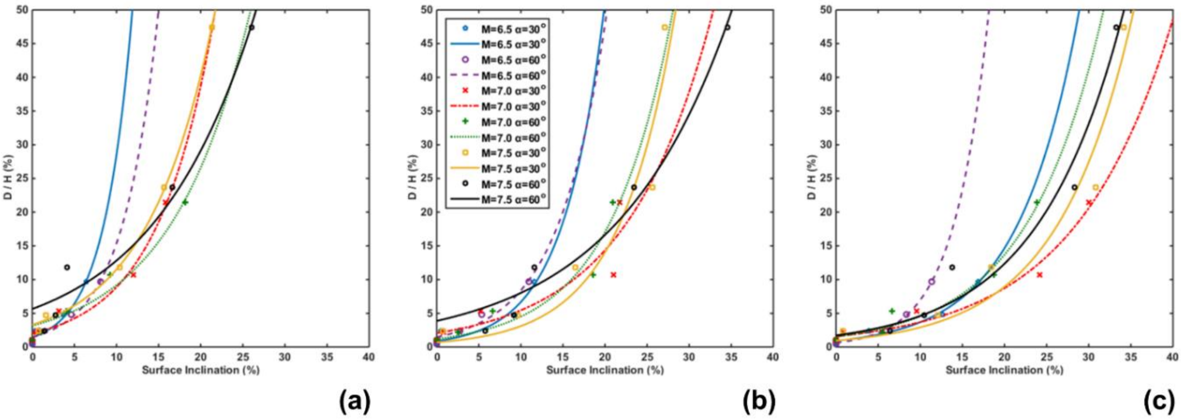

Figure 10: Compressive strains for normal faulting: a) LS, b) MS, and c) DS.

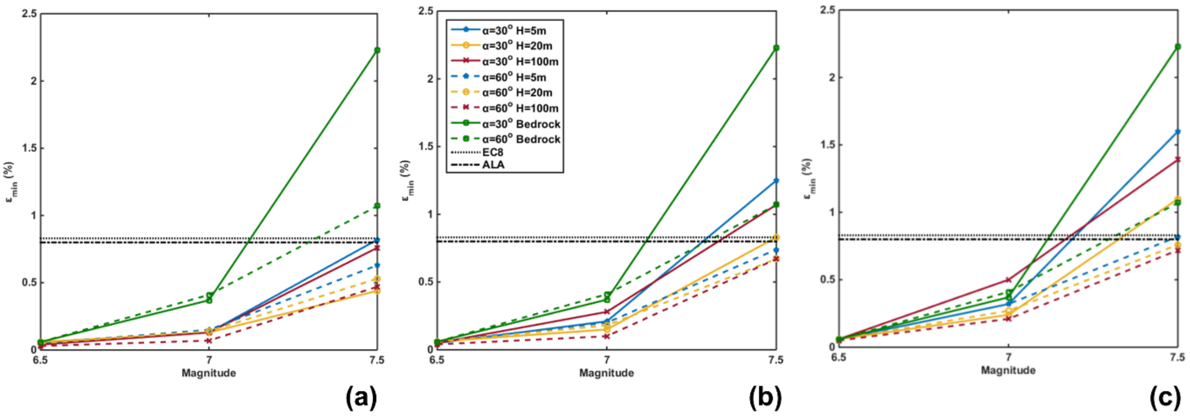

Figure 11: Compressive strains for reverse faulting: a) LS, b) MS, and c) DS.

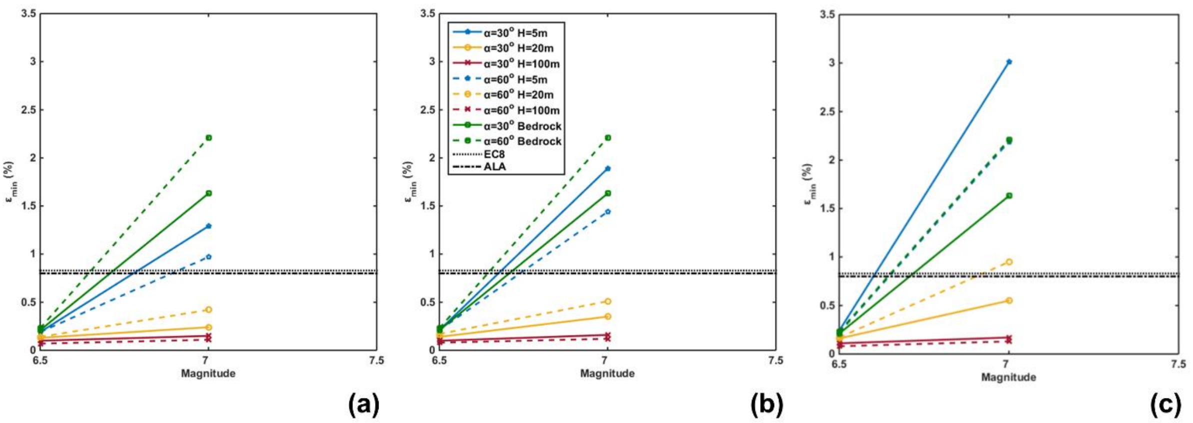

So far pipeline distress has been examined neglecting the presence of internal pressure and temperature variation. Therefore, Figure 12a reveals that a typical internal pressure, i.e., P_{int} = *14 MPa*, prevents the occurrence of local buckling. Additionally, the presence of both internal and external pressure has been investigated, which can be considered equivalent to an offshore pipeline simulation, due to the hydrostatic external pressure. Three different external pressures are considered (i.e., *7*, *14*, *21 MPa*) in order to examine the scenarios where $P_{int} > P_{ext}$, $P_{int} = P_{ext}$ *and* $P_{int} < P_{ext}$. Figure 12b demonstrates the significant compressive strains for

$P_{ext} = 21\ MPa$ (i.e., corresponding to a pipeline that is placed *2100 m* below the sea level).

Figure 12: Compressive strains for various pipeline pressures.

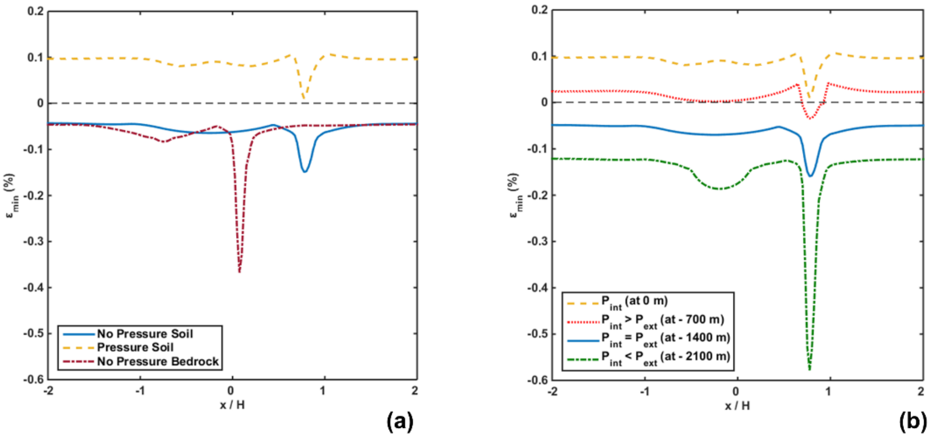

6. CONCLUSIONS

The current study numerically investigates the complex phenomena of seismic fault rupture propagation to ground surface and fault-pipeline intersection. The main aim is to correlate the ground surface inclination, in terms of Permanent Ground Displacements (PGDs), and pipeline kinematic distress, in terms of strains, with earthquake magnitude. For this reason, two decoupled FE models are developed for the analyses of soil response and pipeline distress. Both models have been successfully validated against experimental results. A parametric study of various loading conditions due to normal and reverse faults, as well as soil layer characteristics has been conducted. As a result of this investigation, useful charts have been produced, which can be used for the preliminary seismic design of buried steel pipelines.

The main findings of this investigation can be summarized as follows:

- Sandy deposits consisting of Loose Sand present significantly lower values of both surface inclination and pipe strains compared to Normal and Dense Sands, regardless of earthquake magnitude, thus, having a beneficial impact on pipeline distress (i.e., reduction of maximum absolute value of compressive strains of the order of 60% and 80% for normal and reverse fault, respectively).
- Reverse faulting results in significant decrease of ground surface inclination and pipe strains for a deposit depth H ≥ 20 m, regardless of dip angle value, sand type and earthquake magnitude. This practically means that a pipeline could cross with safety a reverse fault which is covered with medium to thick soil deposits.
- Normal fault dipping at an angle α = 30° results in higher levels of surface inclination (compared to α = 60°), regardless of sand type, soil layer thickness and earthquake magnitude.
- Soil cover subjected to 60°-normal-faulting prevents the pipe from exceeding the allowable limits of both tensile and compressive strains for all the examined earthquake magnitudes for all sand types.

Conclusively, pipelines that are laid directly on bedrock when subjected to excessive fault ruptures (i.e., for high earthquake magnitudes) usually exhibit large strain levels. On the other hand, the presence of thick soil deposits over the rigid bedrock usually reduces pipeline distress. However, the presence of thin-to-medium soil strata increases the complexities of fault rupture propagation and fault-pipeline intersection, which should be examined more thoroughly on a case-by-case basis, taking into account all main parameters involved (i.e., soil, fault, as well as pipeline characteristics).

REFERENCES

American Lifelines Alliance, 2001. Guidelines for the design of buried steel pipes. American Society of Civil Engineers, Reston, VA.

Anastasopoulos, I., Gazetas, G., Bransby, M.F., Davies, M.C.R., El Nahas, A., 2007. Fault rupture propagation through sand: Finite-element analysis and validation through centrifuge experiments. J. Geotech. Geoenv. Eng. 133, 943–958. https://doi.org/10.1061/(asce)1090-0241(2007)133:8(943)

Bonilla, M.G., Mark, R.K., Lienkaemper, J.J., 1984. Statistical relations among earthquake magnitude, surface rupture length, and surface fault displacement. Bull. Seismol. Soc. Am. 74, 2379–2411. https://doi.org/https://doi.org/10.1785/BSSA0740062379

Bray, J.D., 1990. The Effects of tectonic movements on stresses and deformations in earth embankments. University of California, Berkley, CA, USA.

Bray, J.D., Seed, R.B., Cluff, L.S., Seed, H.B., 1994. Earthquake fault rupture propagation through soil. J. Geotech. Eng. 120, 543–561. https://doi.org/10.1061/(ASCE)0733-9410(1994)120:3(543)

Chang, Y.Y., Lee, C.J., Huang, W.C., Hung, W.Y., Huang, W.J., Lin, M.L., Chen, Y.H., 2015. Evolution of the surface deformation profile and subsurface distortion zone during reverse faulting through overburden sand. Eng. Geol. 184, 52–70. https://doi.org/10.1016/j.enggeo.2014.10.023

Chatzidakis, D., Tsompanakis, Y., Psarropoulos, P.N., 2022. Kinematic distress of pipelines subjected to secondary seismic fault rupture. Soil Dyn. Earthq. Eng. 152, 107065. https://doi.org/10.1016/j.soildyn.2021.107065

Simulia, 2014. Abaqus 6.14 Anal. User's Guid. Dassault Systèmes.

European Commitee for Standardization (CEN), 2006. EN 1998-4:2006 - Eurocode 8: Design of structures for earthquake resistance - Part 4: Silos, tanks and pipelines.

Fadaee, M., Farzaneganpour, F., Anastasopoulos, I., 2020. Response of buried pipeline subjected to reverse faulting. Soil Dyn. Earthq. Eng. 132, 106090. https://doi.org/10.1016/j.soildyn.2020.106090

Jalali, H.H., Rofooei, F.R., Khajeh, A.A.N., 2018. Performance of buried gas distribution pipelines subjected to reverse fault movement. J. Earthq. Eng. 22, 1068–1091. https://doi.org/10.1080/13632469.2016.1269694

Joshi, S., Prashant, A., Deb, A., Jain, S.K., 2011. Analysis of buried pipelines subjected to reverse fault motion. Soil Dyn. Earthq. Eng. 31, 930–940. https://doi.org/10.1016/j.soildyn.2011.02.003

Karamitros, D.K., Bouckovalas, G.D., Kouretzis, G.P., 2007. Stress analysis of buried steel pipelines at strike-slip fault crossings. Soil Dyn. Earthq. Eng. 27, 200–211. https://doi.org/10.1016/j.soildyn.2006.08.001

Karamitros, D.K., Bouckovalas, G.D., Kouretzis, G.P., Gkesouli, V., 2011. An analytical method for strength verification of buried steel pipelines at normal fault crossings. Soil Dyn. Earthq. Eng. 31, 1452–1464. https://doi.org/10.1016/j.soildyn.2011.05.012

Kennedy, R.P., Chow, A.M., Williamson, R.A., 1977. Fault movement effects on burried oil pipeline. ASCE Transp Eng J. https://doi.org/10.1061/tpejan.0000659

Loukidis, D., Bouckovalas, G.D., Papadimitriou, A.G., 2009. Analysis of fault rupture propagation through uniform soil cover. Soil Dyn. Earthq. Eng. 29, 1389–1404. https://doi.org/10.1016/j.soildyn.2009.04.003

Nair, G.S., Dash, S.R., Mondal, G., 2018. Review of pipeline performance during earthquakes since 1906. J. Perform. Constr. Facil. https://doi.org/10.1061/(asce)cf.1943-5509.0001214

Newmark, N.M., Hall, W.J., 1975. Pipeline design to resist large fault displacement. Proc. of U.S. Nat. Conf. on Earthq. Eng., pp. 416-425

Oettle, N.K., Bray, J.D., 2017. Numerical Procedures for Simulating Earthquake Fault Rupture Propagation. Int. J. Geomech. 17, 04016025. https://doi.org/10.1061/(asce)gm.1943-5622.0000661

Thebian, L., Sadek, S., Najjar, S., Mabsout, M., 2018. Normal fault movement propagation in overlying seabed deposits. Sustain. Civ. Infrastr. 206–219. https://doi.org/10.1007/978-3-319-61648-3_14

Tsatsis, A., Loli, M., Gazetas, G., 2019. Pipeline in dense sand subjected to tectonic deformation from normal or reverse faulting. Soil Dyn. Earthq. Eng. 127, 105780. https://doi.org/10.1016/j.soildyn.2019.105780

Turgut, A., Isik, N.S., Kasapoglu, K.E., 2017. A new empirical equation proposed for the relationship between surface rupture length and the earthquake source parameters. Bull. Eng. Geol. Environ. 76, 383–392. https://doi.org/10.1007/s10064-016-0960-9

Wells, D.L., Coppersmith, K.J., 1994. New empirical relationships among magnitude, rupture length, rupture width, rupture area, and surface displacement. Bull. Seismol. Soc. Am. 84, 974–1002.